Gap-Junctional Single-Channel Permeability for Fluorescent Tracers in Mammalian Cell Cultures

Reiner Eckert
Abteilung Biophysik, Biologisches Institut, Universität Stuttgart, Stuttgart, Germany

ABSTRACT We have developed a simple dye transfer method that allows quantification of the gap-junction permeability of small cultured cells. Fluorescent dyes (calcein and Lucifer yellow) were perfused into one cell of an isolated cell pair using a patch-type micropipette in the tight-seal whole cell configuration. Dye spreading into the neighboring cells was monitored using a low-light charge-coupled device camera. Permeation rates for calcein and Lucifer yellow were then estimated by fitting the time course of the fluorescence intensities in both cells. For curve fitting, we used a set of model equations derived from a compartment model of dye distribution. The permeation rates were correlated to the total ionic conductance of the gap junction measured immediately after the perfusion experiment. Assuming that dye permeation is through a unit-conductance channel, we were then able to calculate the single-channel permeance for each tracer dye. We have applied this technique to HeLa cells stably transfected with rat-Cx46 and Cx43, and to BICR/M1R_k cells, a rat mammary tumor cell line that has very high dye coupling through endogenous Cx43 channels. Scatter plots of permeation rates versus junctional conductance did not show a strictly linear correlation of ionic versus dye permeance, as would have been expected for a simple pore. Instead, we found that the data scatter within a wide range of different single-channel permeances. In BICR/M1R_k cells, the lower limiting single-channel permeance is $2.2 \pm 2.0 \times 10^{-12}$ mm^3/s and the upper limit is 50×10^{-12} mm^3/s for calcein and $6.8 \pm 2.8 \times 10^{-12}$ mm^3/s and 150×10^{-12} mm^3/s for Lucifer yellow, respectively. In HeLa-Cx43 transfectants we found $2.0 \pm 2.4 \times 10^{-12}$ mm^3/s and 95×10^{-12} mm^3/s for calcein and $2.1 \pm 6.8 \times 10^{-12}$ mm^3/s and 80×10^{-12} mm^3/s for Lucifer yellow, and in HeLa-Cx46 transfectants $1.7 \pm 0.3 \times 10^{-12}$ mm^3/s and 120×10^{-12} mm^3/s for calcein and $1.3 \pm 1.1 \times 10^{-12}$ mm^3/s and 34×10^{-12} mm^3/s for Lucifer yellow, respectively. This variability is most likely due to a yet unknown mechanism that differentially regulates single-channel permeability for larger molecules and for small inorganic ions.

INTRODUCTION

Gap junctions are specialized membrane structures that consist of clusters of cell cell channels. These channels mediate fast exchange of low-molecular-weight components between directly adjacent cells. Gap-junctionally coupled cells, therefore, act as a functional syncytium for ions, second messengers, and metabolites without compromising their cellular integrity at a higher level.

The high-molecular-weight cut-off for permeation has traditionally been utilized to demonstrate that cells can communicate via gap-junction channels: fluorescent dyes (e.g., Lucifer yellow) were injected into the cytoplasm of one cell of a cell cluster. If gap junctions were present, dye spreading into neighboring cells could be observed (1,2). Iontophoretic injection of different fluorescent molecules has also been used to estimate gap-junction channel size via their molecular cut-off at ~800 Da or 1.4- to 1.6-nm pore diameter (3–5).

More recently, the identification of a large number of gap-junction proteins, the connexins (6), has focused interest toward the functional consequences of this connexin diversity. Electrophysiological characterization has shown that different connexin isoforms indeed confer different functional properties to gap-junction channels, e.g., different single-channel conductance and voltage sensitivity. However, it is now widely considered that the permeability properties of gap-junction channels are equally or even more important for tissue function than their electrical properties (7–10). This has led to a reevaluation of some of the early dye-transfer studies with respect to the role of connexin composition of the gap junction channels involved (7,8,11–14).

These studies have demonstrated qualitatively that there are significant selectivity differences between different connexin isoforms. However, quantitative data on gap-junction permselectivity, particularly single-channel permeabilities for larger molecules, which would be comparable between different connexin isoforms, are not widely available (8). The reason for this is partially technical in nature. There have been a number of reports that have addressed the quantification of dye spreading in either linear (15–17) or two-dimensional cell arrangements (18–20). However, calibration and analysis of these experiments were technically demanding, so that the possibility of obtaining comprehensive studies on different dyes and/or channel types was limited. It is also worth noting that whereas most of these studies provided values for the permeability of gap-junction membranes, they fell short of relating these to single channels by not providing additional estimates on channel number.

To address this problem, Cao et al. (14) have performed correlated measurements of dye transfer and gap-junctional

Submitted August 10, 2005, and accepted for publication April 6, 2006.

Address reprint requests to Reiner Eckert, Abteilung Biophysik, Biologisches Institut, Universität Stuttgart, Pfaffenwaldring 57, D-70550 Stuttgart, Germany. Tel.: 49-711-6856-5030; Fax: 49-711-6856-5096; E-mail: reiner.eckert@bio.uni-stuttgart.de.

© 2006 by the Biophysical Society

0006-3495/06/07/565/15 $2.00

doi: 10.1529/biophysj.105.072306

conductance in connexin-transfected HeLa cells and *Xenopus* oocytes. This was one of the first studies to relate permeability measures to channel number. However, it still suffered from a few shortcomings. One of the tracer dyes, DAPI (4′,6-diamidino-2-phenylindole), is only visible after binding to DNA and might be considered inadequate as a diffusion tracer. In addition, the permeability was estimated by counting the number of cells that had received dye after a specified period of time. However, counting cells depends on an arbitrary threshold of fluorescence intensity (visibility) and will be different for different tracer dyes. The cell count is also not linearly related to junctional permeability, and, therefore, arguably an inaccurate measure. In an extension of this work, Weber et al. (21) used the experimental techniques established for *Xenopus* oocytes and applied diffusion modeling to obtain quantitative single-channel permeability data. Using this approach, they were able to provide quantitative values for the permeability of a number of connexins and a set of structurally similar dyes (21,22).

A similar approach using mammalian cells was used by Valiunas et al. (23), who used dye perfusion into isolated HeLa cell pairs to quantify dye flux through single Cx40 and Cx43 gap-junction channels. Here, we report an extension of this technique, where we have adapted compartment models (24) to model the time course of dye transfer between isolated cell pairs perfused via a patch pipette. Using these models, we were able to obtain quantitative estimates of gap-junctional permeance in conjunction with total junctional conductance from the same cell pair. This way we were able to quantify single-channel permeabilities for defined connexin channels in mammalian cells.

MATERIALS AND METHODS

Cell culture

BICR/M1R$_k$ cells (ECACC No. 96112021) are a permanently growing cell line derived from a mammary tumor of the Marshal rat. HeLa DH cells (ECACC No. 96112022) that were stably transfected with rat Cx43 and rat Cx46 were a gift of Drs. C. Elfgang, O. Traub, and K. Willecke (Universität Bonn). Cells were cultivated in Dulbecco's modified Eagle's medium (DMEM) containing 10% newborn calf serum in a humidified CO_2 incubator at 37°C, according to standard cell culture procedures. Media for HeLa transfectants were additionally supplemented with 1 μg/ml puromycin (Sigma, Deissenhofen, Germany) for selection.

For dye transfer measurements, cells were grown as monolayers in small petri dishes (36-mm diameter, Greiner, Frickenhausen, Germany). Immediately before the experiments, cells were briefly treated with trypsin (3 min), replated on 12-mm round glass coverslips (Hecht-Assistent, Sondheim/Rhön, Germany), and left to adhere for 20 min before placing the coverslips into a perfusion chamber with phosphate-buffered saline solution adjusted to 340 mOsM/kg with sucrose.

Electrophysiology and image recording

For the dye-perfusion experiments, low-resistance patch pipettes were pulled from soda-lime glass capillaries (No. 564 microhematocrit nonheparinized, Hecht-Assistent) to a final resistance of 2–5 MΩ using a vertical pipette puller (L/M-3P-A, List Medical, Darmstadt, Germany) and backfilled with standard intracellular pipette solution (140 mM KCl, 2 mM $MgCl_2$, 10 mM K_2EGTA, 10 mM HEPES, pH 7.4). For perfusion experiments with calcein, 500 μM calcein (Sigma) were added to this solution. For Lucifer yellow perfusion, the pipette solution was saturated with the dipotassium salt of the dye (Sigma) and used directly for the experiments. Structure and molecular dimensions of the two tracer dyes are shown in Fig. 1.

Pipettes were mounted into the holder of two patch-clamp amplifiers (EPC-7, EPC-8, Heka Elektronik, Lambrecht, Germany) with their headstages attached to two Leitz mechanical micromanipulators (Leitz, Wetzlar, Germany). Cells were visualized using an inverted microscope (Fluovert, Leitz) with long-distance EF-L 32×/NA 0.40 phase-contrast objective and epifluorescence optics (filter sets L3: ex BP450-490; bs 520; em BP525/20 for calcein and E3: ex BP436/7; bs 475; em LP490 for Lucifer yellow fluorescence, respectively). A low-light charge-coupled device (CCD) camera (VCAMBW, WPI, Berlin, Germany) was attached to the camera port of the microscope and interfaced to the computer by a monochrome frame grabber (DataTranslation, Bietigheim-Bissingen, Germany).

Standard whole cell recording techniques (25) were used to perfuse a single cell of an isolated cell pair with the dye solution. During the perfusion experiments, a series of images were captured at 10-s intervals using Axon Imaging Workbench 4.0 imaging software (Axon Instruments, Foster City, CA). The first image of a sequence was always taken with phase-contrast illumination to obtain a clear definition of the location and size of each cell. After switching off the bright field illumination, several image cycles were passed before breaking the patch-membrane to obtain a well defined baseline and starting point for the perfusion time series. No iontophoretic current was used in these experiments, and all experiments were carried out at room temperature.

To minimize photobleaching of the dyes and exposure of the cells to ultraviolet light, a mechanical shutter (Leitz) was fitted into the ultraviolet-illumination pathway, which was switched open from 0.2 s before to 0.2 s after image capture by the imaging program. During each cycle, two frames were captured from the video camera at video rate (25 Hz) into the frame buffer and averaged by the image acquisition program to reduce image noise.

Gap-junctional conductance was recorded immediately after the perfusion experiments with a second patch pipette. Current signals were low-pass filtered using two eight-pole Bessel filters (Frequency Devices, Haverhill, CA) and fed with their corresponding voltage signals into the inputs of a Digidata computer interface (Axon Instruments), which was used for data recording and generation of voltage waveforms controlled by the Clampex 8 software (pClamp 8, Axon Instruments). Pulse protocols used for recording are shown (see Fig. 6). Total junctional conductance was estimated from linear fits to the *I*/*V* curves generated from the records using Clampfit 8.

Camera and image calibration

The low-light CCD camera we used for image capture has a built-in gamma factor that distorts the linear relationship of image light intensity and

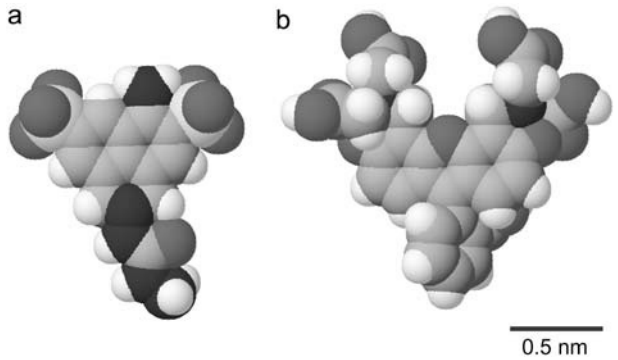

FIGURE 1 Structure of the two fluorescent tracer dyes Lucifer yellow (*a*) and calcein (*b*).

gray-scale value. For quantitative imaging, this must be corrected using a camera density calibration curve. We used UTHSCSA ImageTool (http://ddsdx.uthscsa.edu/dig/) for postprocessing of the image series. This program provides built-in density calibration using a lookup table of gray-scale values versus densities, e.g., from a calibrated optical density standard. We measured camera calibration curves of fluorescence intensity versus dye concentration for each dye using series dilutions of the dye test solutions. A small amount (10 μl) of test solution was spotted onto a test slide made from a microscopic-slide, double-sided adhesive tape (Tesa Fotostrip, Beiersdorf, Hamburg, Germany), and a 24 × 60-mm glass coverslip. The adhesive tape was attached to a microscope slide and a glass coverslip was placed on top of the tape that now serves as a spacer with ~50-μm thickness. For each dye concentration, a series of five images was taken from different regions within the test channels, plus one (dark) background image series of a channel containing buffer only. The mean gray-scale value was calculated over the whole image area for each of the images. For the calibration curves, gray-scale densities for each test image were corrected for background (e.g., dark current of the CCD) by subtracting the density of the corresponding background image and plotted against the relative dye concentration. These values were entered into the calibration table of the imaging program. The table was then saved as a calibration file that was applied to any of the subsequent images.

In addition to the density calibration, we also used spatial calibration for the microscopic images. Similar to the procedures for density calibration for each objective of the microscope, two images of a microscale slide (Zeiss, Oberkochen, Germany) were taken at perpendicular orientation. From these images, scale factors were obtained in *x*- and *y*-directions that translate pixel distances into micrometer-scale values. Again, calibration files were stored to disk for later recall.

Image analysis and quantification of dye diffusion

To obtain the time course of fluorescence intensity, stored image series from Axon Imaging Workbench were converted into TIFF-format image stacks and analyzed off-line, using a macro function written for UTHSCSA ImageTool 3.0.

In brief, the outline of each cell of a cell pair was traced manually in the first (phase-contrast) image of each series. Then the cumulative gray-scale intensity was measured within the two outlined areas for all images in the time sequence. In addition, the mean radius for each area was calculated. The cell volume was then estimated as the volume of a sphere with that radius. The radius is scaled to its correct length (in μm) and the intensities to relative fluorescence intensity using the built-in spatial and densitometric calibration facility of UTHSCSA ImageTool. The cumulative intensities and the cell radius, as well as the mean background intensity for each image, were then stored in tabular format as a text file for further analysis.

Time courses of the fluorescence intensities for different cell pairs were imported into the graphics package Microcal Origin 7.0. Model equations as detailed in the theory section below, were generated using the symbolic differential equation solver of Maple V (Release 4, Waterloo Maple, Waterloo, Canada) and exported as C-functions into Origin-C, the scripting language available for the curve fitter in Microcal Origin. These functions were then fitted to the intensity time course to estimate the permeances κ_{pip} and κ_j for dye transfer in a three-compartment model. The presence of background fluorescence was accounted for either by background subtraction or by the introduction of a constant offset term into the formulae used for curve fitting.

Theory

Tracer diffusion between two cells

For the derivation of analytical solutions for the kinetics of dye uptake into each cell of a perfused cell pair, we modified the compartment model initially proposed by Zimmerman and Rose (24) for analysis of dye transfer in salivary glands of *Chironomus thummi* larva. An outline of the model is shown in Fig. 2.

In this model, there are three compartments—pipette, cell 1, and cell 2—that are coupled by diffusional exchange. The tracer concentration in each compartment can be described by a set of three differential equations.

1st compartment (pipette):

$$\frac{dc_{pip}}{dt} = -k_{bleach}c_{pip}; \tag{1}$$

2nd compartment (perfused cell or cell 1):

$$\frac{dc_1V_1}{dt} = P_{pip}A_{pip}(c_{pip} - c_1) - P_jA_j(c_1 - c_2) - P_1A_1(c_1 - c_{out}) - k_{bleach}V_1c_1; \tag{2}$$

3rd compartment (recipient cell or cell 2)

$$\frac{dc_2V_2}{dt} = P_jA_j(c_1 - c_2) - P_2A_2(c_2 - c_{out}) - k_{bleach}V_2c_2. \tag{3}$$

Here, c_{pip}, c_1, and c_2 are the tracer concentrations in the pipette, the perfused cell (cell 1), and the recipient cell (cell 2), P_j, P_1, and P_2 are the gap-junctional and membrane permeabilities, A_1 and A_2 and V_1 and V_2 are the corresponding cell surface areas and volumes, respectively, and k_{bleach} is the rate constant for photobleaching of the tracer dye.

For image analysis purposes, it is more convenient to describe the two cellular compartments in terms of (molar) number of tracer molecules rather than concentration. Thus, Eq. 2 will be rewritten as

$$\frac{dN_1}{dt} = P_{pip}A_{pip}\left(c_{pip} - \frac{N_1}{V_1}\right) - P_jA_j\left(\frac{N_1}{V_1} - \frac{N_2}{V_2}\right) - P_1A_1\left(\frac{N_1}{V_1} - c_{out}\right) - k_{bleach}N_1 \tag{4}$$

and Eq. 3 will be

$$\frac{dN_2}{dt} = P_jA_j\left(\frac{N_1}{V_1} - \frac{N_2}{V_2}\right) - P_2A_2\left(\frac{N_2}{V_2} - c_{out}\right) - k_{bleach}N_2. \tag{5}$$

The areas A_{pip} and A_j are not accessible experimentally and, therefore, the quantities $P \times A$ will be lumped together into a single constant, the permeance κ with $\mu m^3/s$ units (thus, $\kappa_{pip} = P_{pip} \times A_{pip}$, $\kappa_j = P_j \times A_j$, and so on).

This set of differential equations can be solved using Maple V and will provide analytical solutions for the time course of tracer concentrations in each compartment. These solutions are, however, quite lengthy and will

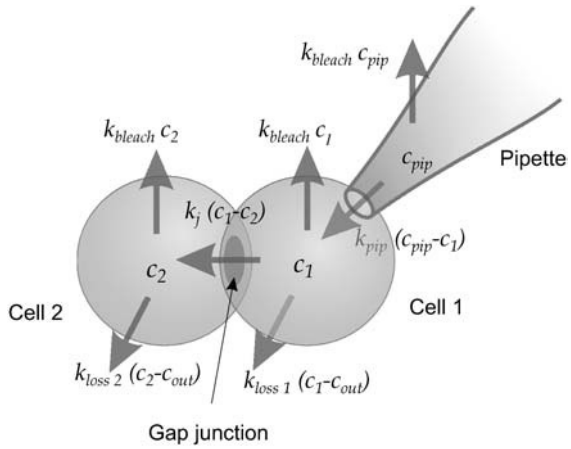

FIGURE 2 Schematic representation of the three-compartment model for dye transfer in a perfused cell pair.

therefore not be included in this text. A commented Maple worksheet with solutions can be obtained at the author's Web site at www.uni-stuttgart.de/bio/biophysik/abteilung/mitarbeiter/reiner_eckert/forschung.en.html.

Geometrical considerations on transfer rate estimates

Fluorescence intensity at low tracer concentration is linearly related to dye concentration and the thickness d of the dye layer (see calibration curves) according to

$$I_F = \varepsilon\, d\, c_{Tracer}, \tag{6}$$

where ε is a dye-specific parameter that depends on, e.g., the quantum efficiency of the tracer dye, its excitation diameter, etc.

Let us now consider the gray-scale intensity distribution of a fluorescence image of a cell that is uniformly filled with tracer dye. This will be

$$I_F(x,y) = \varepsilon\, d(x,y) c_{Tracer}. \tag{7}$$

The cumulative intensity FI over the whole area of the cell is thus

$$\begin{aligned} FI &= \iint_{xy} I_F(x,y) = \iint_{xy} \varepsilon\, d(x,y) c_{Tracer} \\ &= \varepsilon\, c_{Tracer} \iint_{xy} d(x,y) \\ &= \varepsilon\, c_{Tracer} V_{cell}. \end{aligned} \tag{8}$$

Since $c = N/V$ we find that

$$FI = \varepsilon N_{Tracer}. \tag{9}$$

Thus, for image analysis purposes it is more convenient to use the total amount of tracer within a cell for the model equations rather than its concentration, as this quantity is directly proportional to the intensity integral over the area of a cell.

Normalization

The current density ι carried by the ion i through a membrane of area A is

$$\begin{aligned} \iota_i &= \frac{I}{A} = \frac{D_i}{l}\frac{z_i^2 F^2}{RT} c_i U \\ &= P_i \frac{z_i^2 F^2}{RT} c_i U. \end{aligned} \tag{10}$$

From Ohms law we obtain for the conductance

$$\begin{aligned} G_i &= P_i A \frac{z_i^2 F^2}{RT} c_i \\ G_{tot} &= \sum_i P_i A \frac{z_i^2 F^2}{RT} c_i. \end{aligned} \tag{11}$$

Thus, the total conductance (e.g., of a gap junction) should be directly proportional to the permeability for the main charge-carrying ions (predominantly K^+ and Cl^-).

Normalizing the dye permeation constants κ_j to the total junctional conductance G_j is equivalent to

$$\frac{\kappa_j}{G_j} = \frac{P_{dye}}{P_{ions}} \frac{RT}{z_{ions}^2 F^2 c_{ions}}, \tag{12}$$

where the second term is a constant depending on the pipette solutions and the bath temperature. Assuming a linear relationship of κ_j with junctional conductance G_j, the single-channel permeation rate κ_{pore}, as given by Nitsche et al. (22), can be estimated if the single-channel conductance is known. These values are given in units of mm^3/s i.e., a volume transfer rate rather than in units of mm/s for permeabilities. They will therefore be referred to as single-channel ''permeance'' throughout this manuscript. However, these values are proportional to the single-channel permeability by the cross-sectional area of the pore.

RESULTS

Dye calibration

To establish the relation between the gray scale values of the CCD image and dye concentration, we performed calibration measurements with serial dilutions of the tracer. The top row of Fig. 3 shows the calibration curves for the two dyes used in this study. The dilution factors for the dye were 50%, 25%, 20%, 12.5%, 5%, 2.5%, and 0% of the pipette solution, respectively. The logarithmic dependency due to the camera's gamma correction is clearly visible. The lower panel shows the data from the same set of images after automatic intensity calibration. In these graphs, the 100% dye concentration was omitted due to nonlinearities arising from the camera's automatic gain switching. After calibration, the gray-scale readings are linearly dependent on dye concentration with a slope of 1.09 and 0.99 for calcein and Lucifer yellow, respectively. The coefficient of correlation for both dyes was 0.99. The same calibration tables were then used to calculate the total fluorescence intensities in the images obtained from the perfusion experiments.

Time course of dye exchange in isolated cell pairs

For the perfusion experiments, we used isolated cell pairs that were freshly attached to the glass substrate, so that the cells still retained a spherical shape (Fig. 4 *a*). This was necessary to estimate the cell volume, which is a parameter in the equations used for modeling the time course of the tracer perfusion.

After obtaining a gigaseal and rupturing the patch, the tracer concentration inside the attached cell rapidly equilibrates with the tracer concentration in the pipette (Fig. 4). As can be seen in the line scans depicted in Fig. 4 *b*, diffusion within the cell is fast, so that no intensity gradient is evident in the cytoplasm of both cells along the main diffusion axis (Fig. 4, *dotted line*). Therefore, as a first approximation, we can assume the cytoplasm of each cell acts as a well stirred compartment. Fig. 5 shows the time course of the fluorescence intensities of both perfused and neighboring cells for a typical perfusion experiment for calcein (Fig. 5 *a*) and Lucifer yellow (Fig. 5 *b*). The time course in Fig. 5 *a* shows rapid filling of the directly perfused cell, which equilibrates with the pipette within ~200 s. The fluorescence intensity in the neighboring cell lags behind and equilibrium between the cells is reached after ~800 s. In this particular experiment, there is also evidence for some photobleaching, which can be seen as a slight decrease of the intensity in cell 1 after equilibration with the pipette.

Note that in Fig. 5 *b* perfusion appears to be slower than for the calcein experiment, although both pipette and junctional transfer rates from the curve fit appear to be larger.

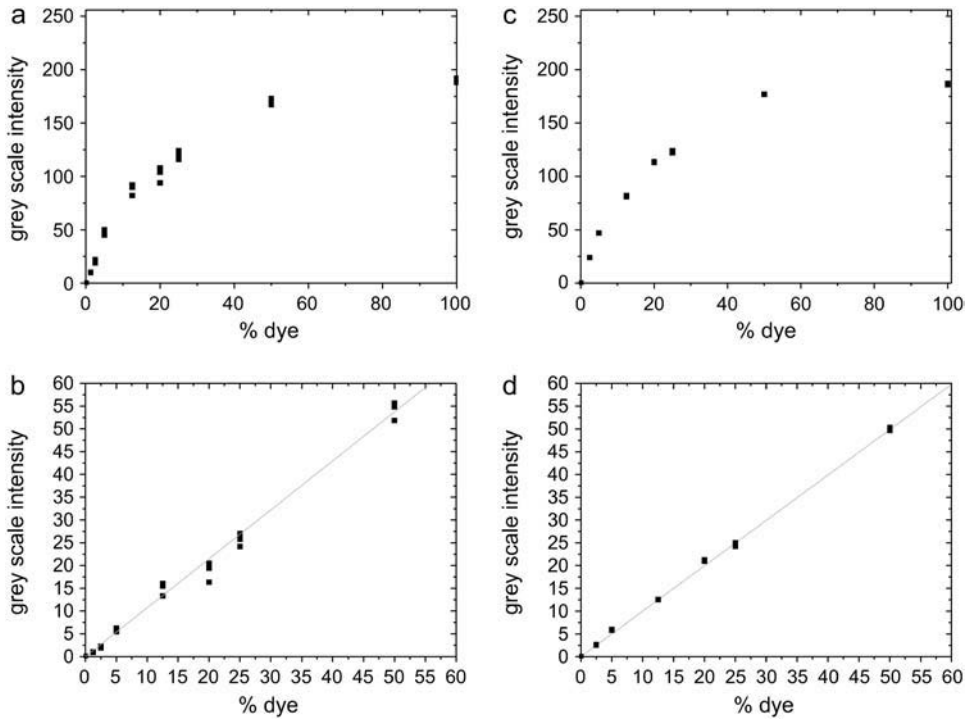

FIGURE 3 Camera calibration curves for calcein (*a* and *b*) and Lucifer yellow concentration (*c* and *d*). (*a* and *c*) Uncalibrated gray-scale intensities for series dilutions of the two tracer dyes. The nonlinearities due to the camera's gamma correction are clearly visible. (*b* and *d*) The same series after correction by the densitometric calibration facility of the image analysis program.

This is due to the different size of the perfused cells. In the experiment shown in Fig. 5 *a*, the cells were smaller (with cell radii of 5.9 μm and 6.3 μm for cells 1 and 2, respectively) than for the experiment in Fig. 5 *b* (cell diameters 8.6 μm and 7.7 μm, respectively).

Although some photobleaching was evident in a number of experiments, we did not observe loss of dye from the cellular compartments except in cases where sealing of the perfusion pipette to the cell was exceptionally bad and the dye would leak through the shunt created by the pipette. These cases could be detected at the start of an experiment by the low-input resistance of the cell and the corresponding experiments were discontinued and discarded from further analysis. Photobleaching was more frequently observed for calcein than for Lucifer yellow. Time constants for bleaching were generally slow, in the range of 30–80 min. In rare cases, we also observed diffusion through cytoplasmic bridges in cell pairs that had undergone incomplete cell division. These could be distinguished from gap-junctional coupling by the transfer of rhodamine-dextran that has a molecular mass of ~17 kDa and is not permeable through gap junction channels (data not shown). These experiments were also excluded from the analysis.

Measurement of gap-junctional conductance

Immediately after the perfusion experiment, the gap-junction conductance was measured using a second patch pipette that was sealed to the second cell (cf. Fig. 4 *a*). After successful sealing, a voltage protocol of two alternating pulses was applied to both cells (Fig. 6 *a*) and the junctional current was determined from the current record in the corresponding nonpulsed cell. The pulse protocol consisted of a series of five test voltages ranging from −20 to +20 mV of transcellular voltage, which was small enough not to elicit any voltage-dependent closure of the channels during the test pulses. The current recordings were then used to create I/V plots (Fig. 6 *b*), from which the junctional conductance was determined by linear regression analysis using the pClamp Clampfit Program. Gap-junctional conductance varied over a wide range from 0 to 95 nS with a mean of 24 ± 20 nS ($n = 78$) for BICR/M1R$_k$ cells, from 0 to 71 nS with mean 11 ± 15 nS ($n = 67$) for HeLa-Cx43 transfectants, and from 0 to 75 nS with mean 11 ± 17 nS ($n = 57$) for HeLa-Cx46 transfectants.

Quantitative estimates of the dye permeance for calcein and Lucifer yellow

For the subsequent analysis, the intensity time courses for both cells were simultaneously fitted with model equations given in the theory section (continuous lines). These were used to estimate the pipette and gap-junctional transfer rates κ_j and κ_{pip}. The model equations also contain additional parameters, such as the starting time of perfusion and the cell radii that were treated as fixed quantities by the fitting routine and were determined separately, e.g., by measurement from the phase-contrast images. Different model equations were used for fitting that allow for additional effects like photobleaching or dye loss through membrane permeabilities, depending on evidence of these effects in the time-course data. The estimation of the junctional transfer rate κ_j proved quite insensitive to the exact choice of model equation and usually did not deviate by >10%.

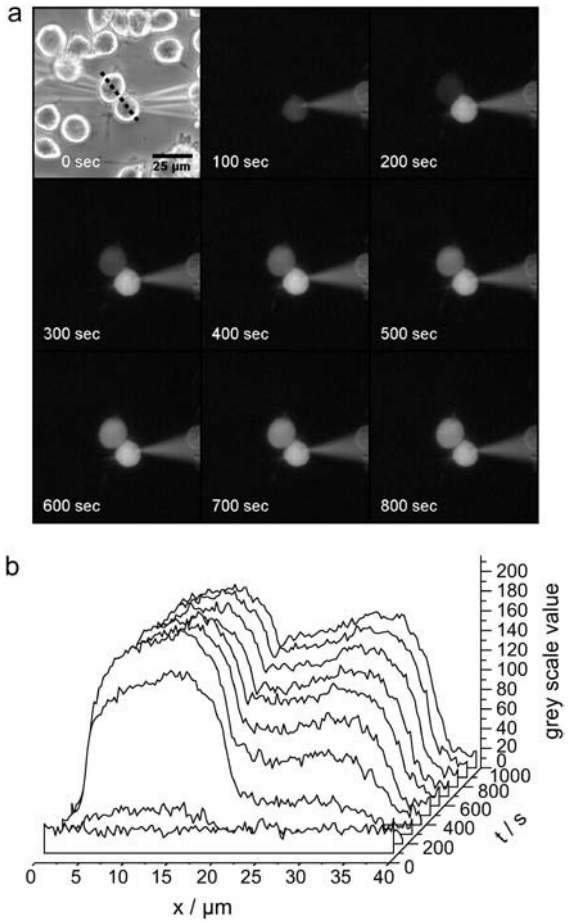

FIGURE 4 Time course of a calcein perfusion experiment in BICR/M1R$_k$ cells. (*a*) Phase contrast and fluorescence images taken at 100-s intervals from a series. (*b*) Evolution of a gray-scale profile taken across the cell pair along the dashed line shown in the phase-contrast image in *a*. Gray-scale values were corrected as shown in Fig. 3 *d*. Equilibration of cell 1 with the perfusion pipette is fast and almost complete within the first two frames shown. There is also no evidence for a diffusion profile within cell 2, indicating that cytoplasmic diffusion is not rate-limiting.

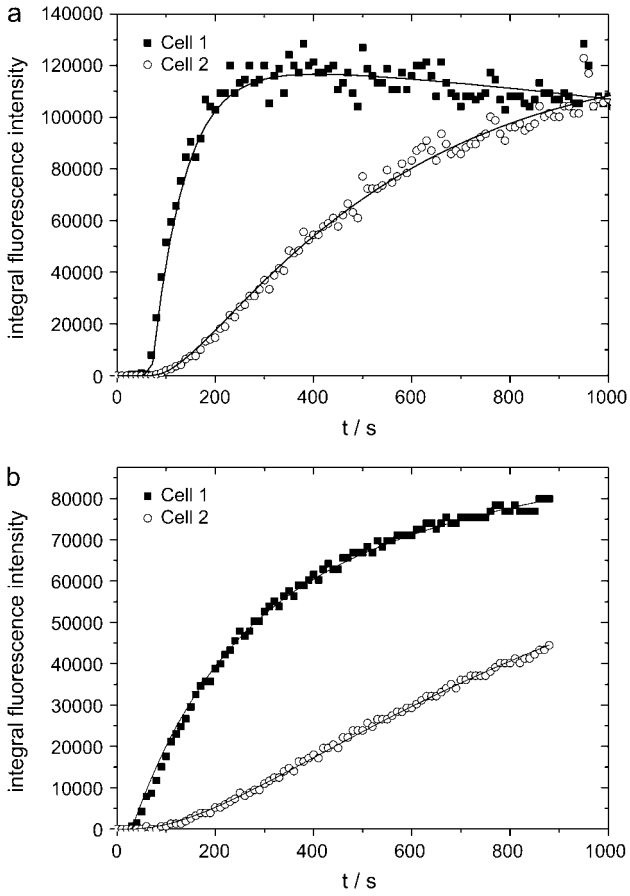

FIGURE 5 Time course of the integrated fluorescence intensities for both cells of a perfused cell pair for calcein (*a*) and Lucifer yellow perfusion (*b*). The solid lines indicate the fits of the diffusion model to the data. The permeation rates are $\kappa_{pip} = 19.6 \pm 1.5$ $\mu m^3/s$ and $\kappa_j = 3.64 \pm 0.09$ $\mu m^3/s$ for the calcein perfusion experiment (*a*) and $\kappa_{pip} = 9.0 \pm 0.3$ $\mu m^3/s$ and $\kappa_j = 2.09 \pm 0.04$ $\mu m^3/s$ for the Lucifer yellow perfusion experiment. Note that the permeabilities are of similar magnitude, although the time course for Lucifer yellow appears slower due to the larger cell volumes in this pair ($cell_1 = 860$ fl and $cell_2 = 1050$ fl in *a* versus $cell_1 = 2650$ fl and $cell_2 = 1900$ fl in *b*). Also note that the fluorescence integral measures the total amount of tracer within a cell. This depends on the cell volume as well as on concentration and, consequently, will not generally be equal once equilibrium has been reached if the cells are asymmetric in size.

The transfer rates obtained by fitting the tracer-intensity time courses of different perfusion experiments were then plotted against the corresponding gap junction conductances measured in the same cell pair immediately after the dye transfer experiments. These data are exemplified in Fig. 7 *a* for calcein transfer in BICR/M1R$_k$ cells. The data shown here represent a total of 65 individual perfusion experiments. As outlined in the theory section, the gap-junctional transfer rate and junctional conductance should be linearly related. One would therefore expect that both quantities should be strongly correlated. However, this is not the case. The coefficient of correlation is $r = 0.61$; that is, there is only weak correlation between the transfer rate and the junctional conductance. The reason becomes apparent in a double-log plot, as seen in Fig. 7 *b*. There the data points seem to cluster into a range bounded by two parallel lines that correspond to channels with a different permeability/conductance ratio, indicating that the variability may be due to the presence of different populations of channels with different permeability properties.

To test whether this heterogeneity also applies to other connexins and cell types, we have included in our analysis two other cell lines: HeLa-Cx43 and HeLa-Cx46 transfectants, which exogenously express rat Cx43 and rat Cx46, respectively. Fig. 8 summarizes the results obtained from all three cell lines. For BICR/M1R$_k$ cells, the data on Lucifer yellow (Fig. 8 *a*) and calcein transfer (Fig. 8 *c*) represent 17 and 63 experiments, respectively. For HeLa-Cx43 transfectants, 26 calcein and 44 Lucifer yellow perfusion experiments were analyzed, and for HeLa-Cx46 transfectants, 25 Lucifer yellow (Fig. 8 *a*) and 20 calcein (Fig. 8 *a*) perfusion experiments were analyzed. Due to the logarithmic scaling, not all data points

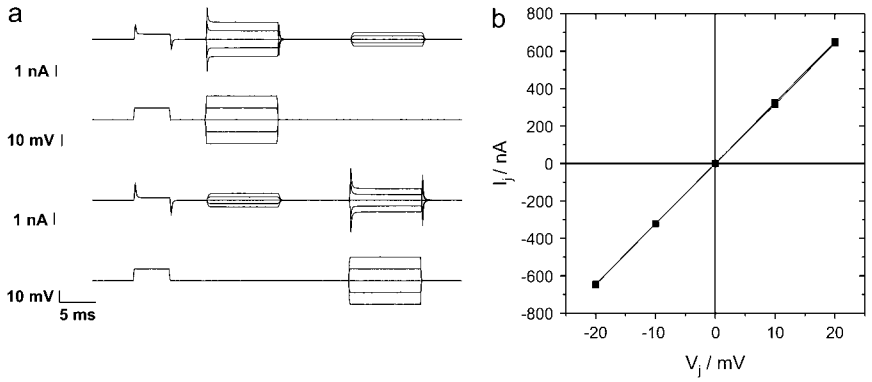

FIGURE 6 Electrophysiological recordings for the determination of the cell-cell conductance. (*a*) Current and voltage recordings from both cells of a cell pair. (*b*) Current-voltage relation of the transjunctional current. The I/V curve was fitted with a straight line where the slope corresponds to the cell-cell conductance.

are shown in these plots. Except for calcein permeance in HeLa-Cx46 transfectants, there appears to be marked scatter in all the plots, indicating that the same mechanism is present in both cell types and for both connexins.

To facilitate comparison with the published values from *Xenopus* oocytes, we have calculated the permeability/conductance ratio for each experiment and rescaled the values as single-channel permeances by normalizing to the single-channel conductance (22). The gap junctions in BICR/M1R_k cells consist of Cx43 with a single-channel conductance of 100 pS for the ionic conditions used in the pipette recording solution (26,27); for Cx46, we used a single-channel conductance of 140 pS ((28), and author's own unpublished observations). Histograms of the single-channel permeance for both dyes are also shown in the right-hand column of Fig. 8. Although the two dyes apparently differ in their permeability relative to each other, a common pattern emerges from these histograms. For both dyes there is a marked peak corresponding to a low but nonzero permeance. In the scatter plots (Fig. 7 and Fig. 8, *left*), this corresponds to a lower-limiting slope indicated by the dotted lines. In addition, there are data points scattered between this lower permeance and a putative maximum limiting permeance that is not readily apparent in the data. The resulting distribution of single-channel permeances is markedly skewed with a large tail toward higher permeance. We have estimated the single-channel permeance corresponding to the lower-limiting slopes seen in Fig. 8 by fitting Gaussian peaks to the histograms (not shown), e.g., in BICR/M1R_k cells we found a single-channel permeance of $\kappa_{pore} = 2.2 \pm 2.0 \times 10^{-12}$ mm^3/s for calcein, corresponding to a slope factor of 0.022 ± 0.02 μm^{3}nS^{-1}s^{-1} in the permeability/conductance plot. The single-channel permeability properties of all cell lines are summarized in Table 1.

Comparison of single-channel dye permeabilities between cell lines

The initial objective of this study was to obtain a permeability measure for gap-junction channels that allows a comparison of channel selectivity for different connexins independent of the cell-type background. To compare the permeabilities between dyes, we plotted the distribution of single-channel permeances versus the Stokes radius and charge of each dye (Fig. 9). Note that the horizontal bars in Fig. 9 correspond to histograms with logarithmic bin widths in accordance with the logarithmic scaling of the ordinate. The Stokes radius was chosen as the main structural determinant of a solute molecule that determines its diffusion constant in bulk aqueous solutions, whereas the tracer charge is most likely the main determinant that dominates long-range interactions of tracer and pore. From these estimates, it appears that in BICR/M1R_k cells, Cx43 gap-junction channels (Fig. 9, *a–d*) are ~2–5 times more permeable to Lucifer yellow than to calcein. However, the statistical range of mean single-channel permeances is much larger within a population of cells for one dye than between dyes.

To test whether this statistical spread depends on the cell background we measured the single-channel permeance in HeLa cells that exogenously express rat Cx43 (Fig. 9, *c* and *d*, and Table 1), i.e., the same connexin isoform as is present in BICR/M1R_k cells (Fig. 9, *a* and *b*). As can also be seen in Fig. 8, the distribution of single-channel permeances of Cx43 channels for calcein in both cell lines appears to be very similar, with almost identical values for the peak permeances and range. On the other hand, the spread for Lucifer yellow is larger in the HeLa transfectants with a large tail toward smaller single-channel permeances. This renders the mean permeance of calcein close to that of Lucifer yellow. The general trend for both distribution profiles appears to be that the smaller tracer Lucifer yellow is similar to or slightly more permeable than the larger calcein. For the HeLa Cx46 transfectants this trend seems to be reversed, with the larger calcein being ~4 times more permeable than Lucifer yellow.

However, as a result of the large variability due to cell background and the very large scatter in the data, it is difficult to show statistically significant trends in the distributions of single-channel permeances that can be attributed to differences between different connexin isoforms.

DISCUSSION

In this study, we present a method for analysis of dye transfer in smaller mammalian cell systems to obtain quantitative

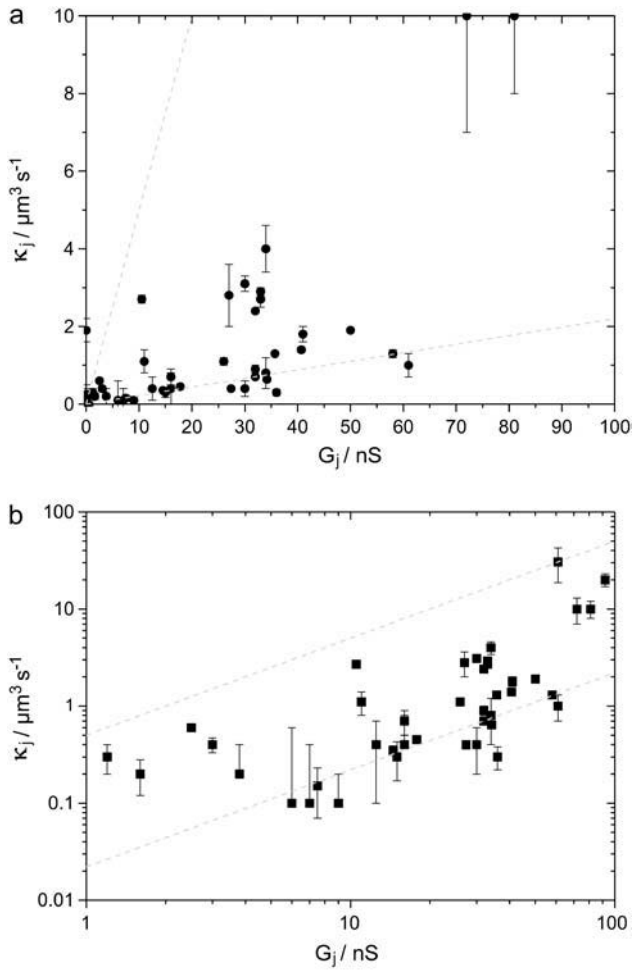

FIGURE 7 Distribution of the dye transfer rates versus cell-cell conductance for calcein in BICR/M1Rk cells shown as (*a*) linear and (*b*) double logarithmic plots. The dashed lines represent the lower-limiting slope corresponding to the peak of the single-channel permeances shown in Fig. 8, below, and a putative upper limit. Note that, due to the double logarithmic scaling in *b*, straight lines through the origin are transformed into parallel lines with the same slope but different offset.

data on specific single-channel permeabilities of gap-junction channels for larger molecules. This was achieved by the combination of a perfusion method described by Valiunas et al. (23) and an adaptation of the compartment model used by Zimmermann and Rose (24). Compartment models were initially used for modeling tracer-dye transfer in *Chironomus* salivary gland. They are as rigorous mathematically as the 3D-diffusion approach presented by Nitsche et al. (22), but less demanding experimentally and with respect to the computer time needed for analysis.

We applied this method to study the transfer of two fluorescent tracers, calcein and Lucifer yellow in BICR/M1R$_k$ cells, a rat mammary tumor cell line that is coupled through Cx43 gap-junction channels. These cells were chosen because due to their very high rate of dye coupling they would serve as a good model system for an initial characterization of the analysis procedure and to establish a permeability profile for Cx43 channels. In addition, we have included HeLa-Cx43 and HeLa-Cx46 transfectants that exogenously express one homologous and one heterologous connexin isoform in a different cell background.

Experimental and analysis procedures

For the main part, single-channel permeabilities were determined using paired *Xenopus* oocytes. This is a widely used system for heterologous expression and electrophysiological characterization of connexins. *Xenopus* oocytes are large cells, and handling and insertion of up to three microelectrodes per cell for combined microinjection and voltage-clamp studies is therefore comparatively simple. On the other hand, the use of small mammalian cells has some advantages over the much larger *Xenopus* oocytes. Specifically the smaller scale of a mammalian cell system simplifies the procedures required for quantitative permeability measurements. Unlike *Xenopus* oocytes, these cells are completely translucent, so there will be minimal loss of fluorescent intensity information due to absorption or scattering. For most of the fluorescent probes there will also be minimal background fluorescence, enhancing the detection sensitivity of the method and lessening the requirements for equipment such as CCD cameras or microscope optics.

Due to the smaller volume of the cells, they fill rapidly with dye and equilibration between the cells can usually be observed within 30 min. This allows perfusion of a cell via a patch pipette by diffusion only, without the use of additional driving forces such as iontophoretic current that could affect gap-junctional coupling. With this procedure, the standard length of our perfusion experiments was set to 10 min. This time was well within the time range during which cells tolerated double whole cell recording without significant deterioration of junctional coupling ($>$30 min). Perfusion via a patch pipette also has the advantage of placing fewer restrictions on the chemical nature of the tracer, and thus the range of possible probes will be larger, including polar and zwitterionic dyes.

For small volumes, cytoplasmic diffusion of the dyes is fast compared to the permeation process through the pipette tip and gap junction. The cytoplasm can therefore be treated as a well-stirred volume, which simplifies the mathematical treatment of the problem. In this case, cytoplasmic diffusion is negligible, and the transport equations can be treated as a set of ordinary differential equations representing three compartments that are coupled by permeances κ (24,29). We have modified the compartment model proposed by Zimmerman (29) for the situation of an isolated cell pair, equilibrating with a single pipette that serves as an infinite source of tracer dye.

By assuming diffusion-driven dye perfusion from a tightly sealed pipette, we can formulate a set of initial conditions for which the differential equations can be solved analytically. These solutions describe the time course of dye concentration

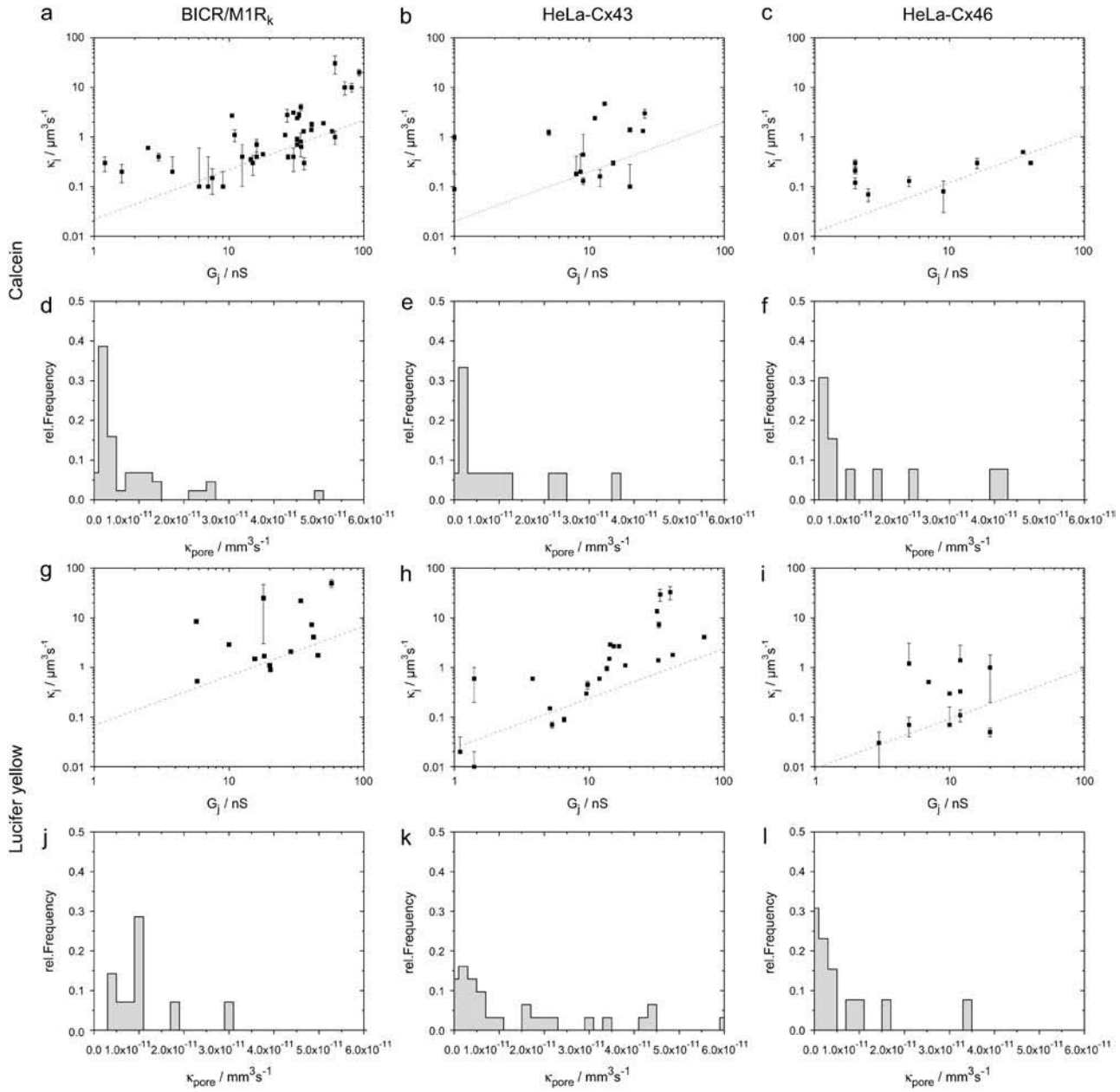

FIGURE 8 Double-logarithmic plots of dye transfer rates versus cell-cell conductance and histograms of the distribution of the single-channel permeances for calcein (*a–f*) and Lucifer yellow (*g–l*) in BICR/M1Rk cells (*a*, *d*, *g*, and *j*), HeLa-Cx43 transfectants (*b*, *e*, *h*, and *k*), and HeLa Cx46 transfectants (*c*, *f*, *i*, and *l*). The dashed lines in the scatter plots represent the lower-limiting slopes corresponding to the peaks of the corresponding distribution of single-channel permeances shown below. Note that, due to the double logarithmic scaling, straight lines through the origin are transformed into parallel lines with the same slope but different offset. Parameters for the slopes and distributions are given in Table 1.

in both cells and can be used by standard curve-fitting programs to estimate the gap-junctional permeance, $P_j \times A_j$. Although still computationally intensive, Levenberg-Marquardt fitting of the time-course equations considerably lessens the computer time required for analysis. Fitting the full model (including photobleaching and dye loss) to the time-course data shown, e.g., in Fig. 4 takes ~3–4 min on an Intel Pentium III with 450 MHz compared to the 7–12 min reported by Nitsche et al. (22).

Although the experimental procedures employed for dye transfer measurement are conceptionally simple, there are some points that have proven critical to obtain reliable results. In addition, the experimental uncertainty of some of these factors may introduce scatter to the permeance data that may explain some of the variability we have observed. The experiments rely on quantitative fluorimetry to estimate tracer concentration inside a cell. It is therefore important to calibrate the CCD camera and the optical system to provide a

TABLE 1 Permeability properties of gap-junction channels in BICR/M1R$_k$ cells and HeLa transfectants

Cell line	Tracer dye	Slope permeance $\frac{\mu m^3}{nS\,s}$	Single-channel permeance κ_{pore} in mm^3/s			
			Low permeance peak	Mean ± SD	Maximum range	n
HeLa Cx46	Lucifer yellow	0.0092 ± 0.001	$1.28 \pm 1.14 \times 10^{-12}$	$6.2 \pm 9.5 \times 10^{-12}$	34×10^{-12}	13
	Calcein	0.012 ± 0.002	$1.7 \pm 0.3 \times 10^{-12}$	$25 \pm 35 \times 10^{-12}$	120×10^{-12}	13
HeLa Cx43	Lucifer yellow	0.021 ± 0.068	$2.1 \pm 6.8 \times 10^{-12}$	$17 \pm 21 \times 10^{-12}$	80×10^{-12}	29
	Calcein	0.02 ± 0.024	$2.0 \pm 2.4 \times 10^{-12}$	$15 \pm 25 \times 10^{-12}$	95×10^{-12}	15
BICR/M1R$_k$	Lucifer yellow	0.068 ± 0.03	$6.8 \pm 2.8 \times 10^{-12}$	$39 \pm 58 \times 10^{-12}$	150×10^{-12}	14
	Calcein	0.022 ± 0.02	$2.2 \pm 2.0 \times 10^{-12}$	$7.5 \pm 9.5 \times 10^{-12}$	50×10^{-12}	44

linear relation between the intensity measure and the dye concentration. It is not essential to calibrate intensities to absolute concentration, however, as this is a linear scaling factor within the equation and can be removed by normalization, e.g., to the maximum fluorescence of cell 1 during the time course.

Another problem that is probably more pronounced with small cells is photobleaching of the fluorescent tracer. We used a shutter in the excitation path that was controlled by the image acquisition software to minimize exposure of the cells to high-energy excitation light. This decreased bleaching to almost negligible levels.

A major factor in obtaining reliable fits was obtaining good estimates for the cell volume of both cells of a cell pair. Underestimating cell volumes leads to low-quality fits and may alter κ-values by a factor of 2–5. To eliminate these errors, we estimated the volume of each individual cell by measuring its diameter and calculating the volume of a sphere with the equivalent radius. To facilitate this, we adjusted the cell preparation procedures for cell pairs and used only freshly attached cells that were close to spherical in shape. The main errors in our estimation arise from two factors. The cells may elongate, i.e., they may deviate from a circular outline to a more ellipsoid or ovoid outline when viewed from above. Since we use the mean diameter of this outline for volume calculation this would lead to a slight overestimation of the volume of the corresponding sphere versus that of the ellipsoid. The length of the main axes of the ellipsoids never exceeded a ratio of 1:1.3, which in the worst case would result in an overestimation of the cell volume by 17% compared to the true cell volume.

The other factor that is probably more pronounced is reduction of the cell volume due to the flattening of the cells where they adhere on the glass substrate. We estimated the cell height as the distance from glass substrate to the top of the cell using a calibrated focal dial with Nomarski optics (40×; NA 0.65). The ratio of cell diameter to cell height was within a range of 0.3 to 1.1. Again, in the worst case, this would lead to an overestimation of the true volume by ~4.6-fold. However, the mean factor for cell flattening was 0.7 ± 0.2 ($n = 20$); that is, the height of a cell was on average ~70% its diameter and the mean elongation factor was 1.12 ± 0.07 ($n = 15$). Thus, a cell was on average ~12% longer than wide. Based on these data, the cell volume estimation is accurate to within 31%, with a general trend to overestimating the true volume. As this scales linearly with estimates for the transfer rates κ from the fitting procedure, we would expect the true transfer rates to be on average ~25% lower than those given by the fitting procedure.

Another mechanism that could significantly alter the analysis would be binding of the tracers to cytoplasmic components. It is well known that in dye injection experiments, Lucifer yellow, for example, preferentially lights up the nuclei and there is also some evidence for binding to cytoplasmic components (16). Cytoplasmic binding is difficult to treat with our experimental procedure as it generally tends to increase the cytoplasmic concentration in the first cell, thereby slowing the apparent transfer rate by a factor that is roughly inversely proportional to the amount of bound tracer within that cell. If tracer binding is approximately the same in both cells, the time course of this process is indistinguishable from free diffusion with a slower transfer rate. However, binding should result in a significant increase in cytoplasmic tracer concentration in both cells and, therefore, in fluorescence intensity relative to the pipette concentration. In HeLa cells, we found that the average cytoplasmic tracer concentration at the end of our 15-min experiments was 60 ± 42% of the pipette concentration for calcein, and 57 ± 26% for Lucifer yellow; in BICR/M1R$_k$ cells, these values were 122 ± 30% and 89 ± 51%. This is consistent with free diffusion or, in the case of calcein in BICR/M1R$_k$ cells, very low cytoplasmic binding. We have, therefore, not included any binding terms to our fitting equations. The consistently lower values observed in HeLa versus BICR/M1R$_k$ cells probably reflect the error resulting from underestimation of cell volume due to cell flattening as the epitheloid HeLa cells attach more readily to the glass substrate than BICR/M1Rk cells.

Regulation of permeability

Previous studies and theoretical considerations predicted a linear relation of gap-junction permeance (termed $P_j \times A_j$ by Nitsche et al. (22) and κ_j herein) to gap-junctional conductance (8,14,26,30). We therefore intended to use scatter plots of these quantities to estimate a single-channel permeance that could be attributed directly to the channel pore. To our surprise, the scatter of the conductance versus transfer-rate

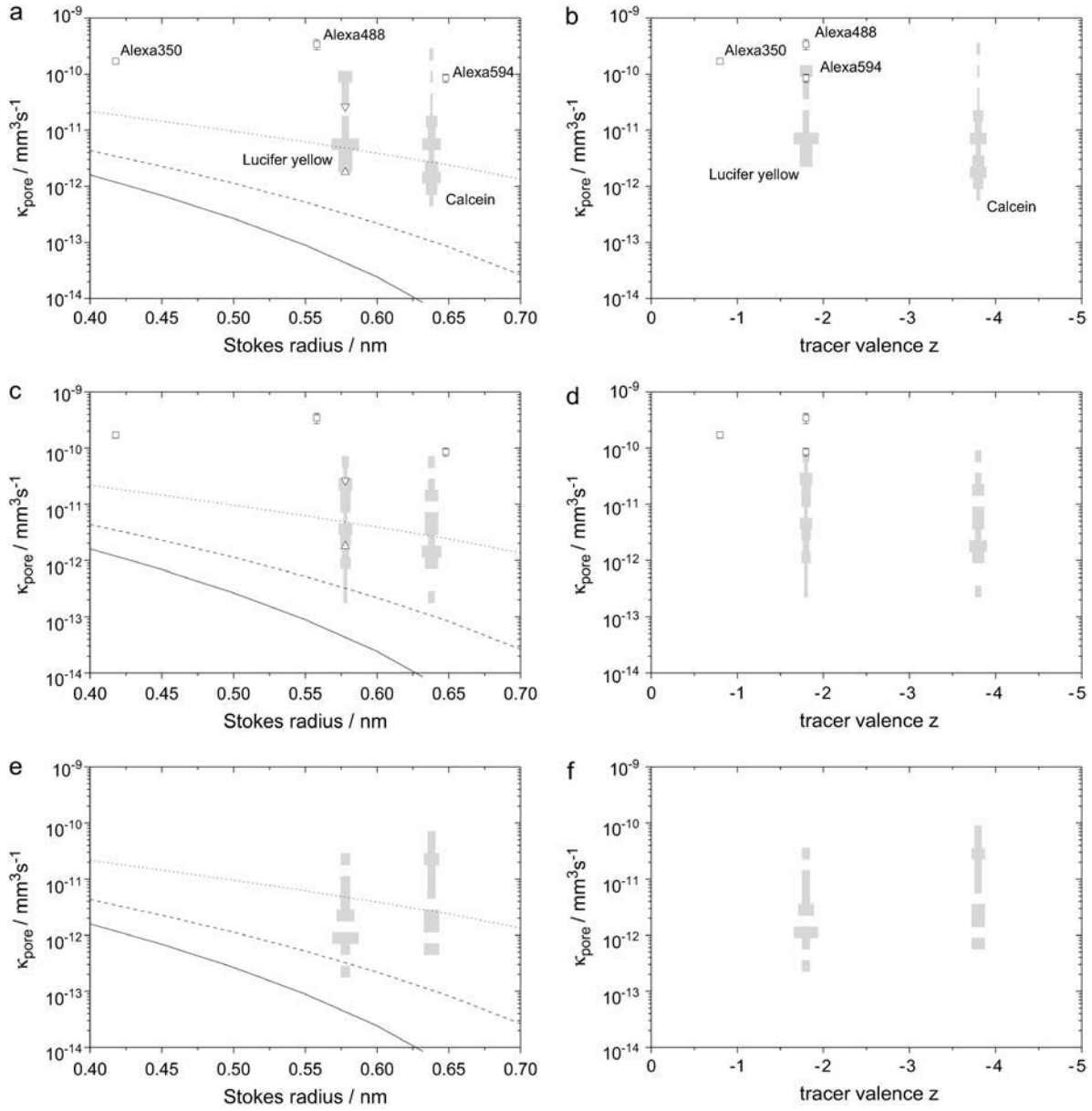

FIGURE 9 Dependence of single-channel permeances on tracer size (*left column*) and charge (*right column*) for BICR/M1R$_k$ cells (*a* and *b*), HeLa-Cx43 transfectants (*c* and *d*), and HeLa-Cx46 transfectants (*d* and *e*). The gray bars represent logarithmic histograms of the distribution of single-channel permeances, with the horizontal width of a bar corresponding to the relative frequency and the vertical width to the bin width of 0.2 $\log_{10}$ units, respectively. The gray lines correspond to the single-channel permeances predicted by a simple model for a straight cylindrical pore of radius 0.74 nm (*solid line*), 0.86 nm (*dashed line*), and 1.19 nm (*dotted line*). The lower bounds of our single-channel permeances are roughly consistent with a simple pore of ~1 nm radius. For reference, we have included data reported by Weber et al. (21) for Alexa-dyes in *Xenopus* oocytes (□) and by Valiunas et al. (23) and Biegon et al. (15) for N2A- (△) and Novikoff hepatoma cells (▽) expressing Cx43 to the BICR/M1R$_k$ and HeLa-Cx43 data sets. Note that for both Lucifer yellow and calcein the range of permeances comes close to the *Xenopus* data, although the maximum values still fall short by a factor of 5–10.

data was much larger than could be expected for a linear relationship (Fig. 7). The easiest way to reconcile the large variability and the comparatively low single-channel permeance of mammalian cells with the *Xenopus* data is if mammalian cells can regulate the permeability of a gap junction for larger organic solutes (determined from the dye transfer rate) more or less independent of its permeability for small inorganic ions (determined from gap-junctional conductance) or vice versa. The different single-channel permeabilities we observed would then represent the average of a population of channels that can occupy two or more different permeability states. The physicochemical nature of this putative regulation mechanism is still not clear. To explain the very high single-channel permeances found in *Xenopus* oocytes by an ab inito pore model, Nitsche et al. (22) introduced an affinity term to their diffusion model. This

assumption seems plausible, since larger solutes can be expected to interact more strongly with the pore structure than small ions. Structural features at the pore wall or at the pore entrance could create preferential ''binding sites'' or energy wells that could enhance partitioning of the solute into the pore.

If we apply the pore models given by Nitsche et al. (22) to our data, the lower-limiting single-channel permeances for Lucifer yellow and calcein would be consistent with a straight cylindrical pore without additional affinities that has a radius of 1.16 nm for Cx43 channels. Although these estimates for the pore radius seem large compared to a pore radius of <0.75 nm from the high-resolution structure (31,32) and 0.63 ± 0.04 nm from ionic permeability data (33), these estimates are still in reasonable agreement with the structural data. It may be interesting to note that the 3D structure was obtained in the presence of ''the sleep-inducing lipid oleamide, which has been shown to induce gap junction closure in vivo'' (31) and therefore represents a closed state that is impermeable for Lucifer yellow (34). On the other hand, even if the maximum ranges of our data are lower than the permeabilities for Alexa dyes, they still cannot be reasonably explained with simple pore models without affinities. Thus, in addition to assuming a gap-junction pore with specific affinities to different solutes, we would also predict in mammalian cells the presence of a yet unknown regulation mechanism that can change these affinities and/or partitioning of the solute into the pore.

This seems likely, as other studies have already reported about differential permeabilities in gap-junction channels and hemichannels depending on channel gating (35,36). From the argument given above, we would also expect that regulation may act on the pore affinities rather than on the pore diameter since the latter would also change the ionic conductance of the pore. It may be tempting to attribute our lower-limiting single-channel permeance to the residual permeability of the channel. In fact, a number of studies have indicated that the stable subconductance state found in almost all gap junction channels to date has different permeability to larger solutes than the fully open state (35,36). However, gating from the main state to this subconductance state is mainly regulated by the transcellular voltage with the main state maximally active at 0 mV. In our experiments, the cells were kept at their normal resting potential. It seems, therefore, unlikely that gating to the substate is responsible for the decrease in single-channel permeance, since there was no voltage difference between the cells.

An alternative explanation may be phosphorylation of the connexin subunits. Nitsche et al. (22) have noted in their discussion that the discrepancies between their data and those from mammalian cells may be accounted for by connexin phosphorylation, which is present in most mammalian cells but not in *Xenopus* oocytes. In cardiac myocytes, treatment with activators of different protein kinases resulted in differential changes in total and single-channel conductances and dye permeabilities for 6-carboxyfluorescein (37) and NBD-methyl-TMA (38) in a manner consistent with the mechanism proposed here. C-terminal phosphorylation would lead to a ring of negative charges around the outer rim of a channel. This would repel anions due to electrostatic screening, decreasing the local concentration of negative solutes at the pore mouth. It is also interesting to note, in this context, that Cx43 in both HeLa-Cx43 transfectants and BICR/M1R$_k$ cells is highly phosphorylated ((27,39), and author's own unpublished observations). Based on gel mobility shift in Western blots of SDS-PAGE of total cell lysates, the amount of phosphorylated protein and the phosphorylation state in both cell lines appears to be similar. However, it is difficult to distinguish, on that basis, what kinases were involved. Phosphorylation via PKA also seems to stabilize junctional Cx43 by decreasing its degradation, thus leading to an overall larger junctional ''activity'' and incidentally a very high rate of dye coupling, which is why we chose the BICR/M1R$_k$ cell line for this study.

Permeability profiles

The initial aim of this study was to provide quantitative permeability profiles for a number of solutes of different size, charge, and structure to probe the properties of a Cx43 gap-junction channel pore. The scattering of the permeance versus conductance data did not allow us to assign a definite single-channel or unit permeability for each connexin-dye combination. However, it may still be possible to deduce some of the factors that govern tracer permeability in different connexins by looking at the distribution of the relative single-channel permeances. Fig. 9 provides an overview of how our data may correlate with some structural factors that have been discussed to affect single-channel permeability of gap-junction channels. These are the size of the tracer relative to the pore diameter (Fig. 9, *a*, *c*, and *e*) and the charge of the tracer molecule (Fig. 9, *b*, *d*, and *f*).

The distribution of single-channel permeances of Cx43 channels in both cell lines (Fig. 9, *a–d*) appears to be similar, with a general trend that the smaller tracer, Lucifer yellow, is slightly more permeable than the larger, calcein. A closer look shows that the lower peaks of the distributions are close to a line that would be predicted for a straight cylindrical pore with a radius of 1.16 nm. Although the number of tracers used in this study is far from exhaustive, this suggests that the lower bound of the tracer permeability in Cx43 is predominantly governed by tracer size and less by charge or long-range electrostatic interactions.

For Cx46 channels this trend seems to be reversed. The larger calcein is ~4 times more permeable than Lucifer yellow. This would be more consistent with a charge preference of the pore. The data shown in Fig. 9 *f* suggest an anion selectivity of Cx46 gap-junction channels. However, this seems inconsistent with the charge selectivity for Cx46 hemichannels, which were reported to be slightly

cation-selective (40). Unfortunately, for Cx46 channels no additional quantitative data for other dyes are available. Therefore, any conclusions on dominance of charge versus size dependence must be considered preliminary, and other factors (like stereoselectivity) cannot be excluded. To answer this question, additional permeability studies using a set of positively charged tracers with similar dimensions would be useful. However, most positively charged tracers that have previously been used as gap-junction tracers (e.g., rhodamine123, DAPI, ethidium, or propidium) either bind to or accumulate in cytoplasmic compartments, which makes them inappropriate for quantitative analysis procedures.

Comparison with other studies

A number of previous studies have reported quantitative data on junctional membrane permeabilities for tracer dyes (16–20,41,42). However, these data were usually raised and interpreted in a tissue context with the main question being how fast and how far a solute will spread in a continuum of cells. For comparison of connexin properties, however, gap-junctional permeability itself is not a good parameter. P_j is a gross property of the junctional membrane and may thus vary with such parameters as channel density and number in this membrane. Technically, it is also easier to measure the gap junction permeance κ, i.e., $P_j \times A_j$, since on most occasions the gap junctional cross-section area A_j is not directly accessible.

So far, there are only a few studies that report quantitative permeability data for channels of defined connexin composition that could be compared to the data presented here. In Novikoff hepatoma, it was possible to correlate the mean cell-cell permeance for Lucifer yellow with mean particle numbers from electron microscopy and to obtain an estimate for the diffusion coefficient within a gap-junction channel (15). In a similar approach, Cao et al. (14) normalized junctional permeability to junctional conductance, which can be used as an estimator for channel number if the single-channel conductivity is known. This would then allow calculation of the single-channel permeance, which is a quantity that could be directly attributed to connexins that constitute the channel pore (8,14,22). Only two of these studies (15,23) were performed in mammalian cell cultures. Unfortunately, neither study provides quantities that could be directly compared to our data. Biegon et al. (15) only provide a single-channel diffusion constant that can be interpreted only when certain assumptions are made about pore diameter and length of a gap-junction channel. Valiunas et al. (23) were primarily interested in transfer of biologically active molecules, and their data is therefore presented in terms of molecules per second, that is, as an (average) particle flux per channel. Although in a physiological context these are meaningful values, this is not a good parameter if one wishes to compare the biophysical properties of different pores. Thus, the only other study that provides compatible data is the one by Weber et al. (21) on the permeabilities of Alexa-type dyes in *Xenopus* oocytes expressing a range of different connexins (21,22). By comparison, the mean single-channel permeances obtained for mammalian cells by Valiunas et al. (23) stick out by being at least two orders of magnitude lower than could be predicted based on the *Xenopus* data.

A direct comparison of our data with the literature values is shown in Fig. 9. The open squares mark the permeabilities found in *Xenopus* oocytes expressing Cx43 gap-junction channels for Alexa-type dyes (21) and the open triangles show the permeabilities for Lucifer yellow in N2A (23) and Novikoff hepatoma cells (15). As can be seen in Fig. 9, our data are consistent with all three previous observations.

Assuming the regulation mechanism discussed above, these reports would represent cells with differential regulation properties. The upper range of single-channel permeances measured in BICR/M1R_k cells approaches the permeabilities for Alexa dyes found in *Xenopus* oocytes. The permeability value of 37×10^{-12} mm^3/s reported for Lucifer yellow in Novikoff hepatoma cells (15) also falls well within the upper range of the distribution found in BICR/M1R_k and HeLa cells. We would therefore conclude that the permeabilities reported in Weber et al. (21) and Biegon et al. (15) are close to, or directly represent, the upper limit or a ''permissive'' state of single-channel permeability.

On the other hand, the lower limit for single-channel permeance (the lower limiting slope of the plot in Fig. 7) for Lucifer yellow in BICR/M1R_k cells is $6.8 \pm 2.8 \times 10^{-12}$ mm^3/s and that for HeLa-Cx43 transfectants is $2.1 \pm 6.8 \times 10^{-12}$ mm^3/s, which are in close correspondence to the permeability value of 2.5×10^{-12} mm^3/s that can be estimated from the report of Valiunas et al. (23) for Lucifer yellow in N2A cells. These permeabilities would then represent a low-limit or ''restricted'' state of single-channel permeability.

The available data are consistent with the assumption that gap-junction channels contain affinity sites that could be masked or created either by structural rearrangement (i.e., gating) or posttranslational modification of the protein (e.g., phosphorylation). So far, the data are inconclusive as to whether affinity sites are created by something like exposure of positive charges at the pore mouth (in the case of a negatively charged solute like calcein), or whether affinity to the solute is a basic property of the pore that is down-regulated by, e.g., shielding of charged residues in the pore wall. Physiologically, the latter scenario seems to be preferable, as the capability of fast downregulation of junctional permeability provides a very effective means for modulation of cell-to-cell signaling (43).

It has been noted by both Valiunas et al. (23) and Nitsche et al. (22) that the junctional permeabilities found in mammalian cells appear too low to be effective for cell-cell signaling with physiologically active molecules that have only a limited lifetime. Our data would suggest that mammalian cells may operate their gap junctions at flux rates that differ by

at least two orders of magnitude. The results from HeLa cells that express Cx46 indicate that this may be a common feature for gap-junction channels in mammalian cell systems.

We thank Ms. Dagmar Mvondo for expert technical assistance, and Ms. Melissa Poynor and Mr. Simon Stutz for critical reading of the manuscript. We are also indebted to the anonymous reviewers for their numerous valuable suggestions to improve this manuscript.

This work was supported by the Deutsche Forschungsgemeinschaft grant Ec 141/6-1.

REFERENCES

1. Stewart, W. W. 1978. Functional connections between cells as revealed by dye-coupling with a highly fluorescent naphthalimide tracer. *Cell.* 14:741–759.
2. Mobbs, P., D. Becker, R. Williamson, M. Bate, and A. Warner. 1994. Techniques for dye injection and cell labeling. *In* Microelectrode Techniques. The Plymouth Workshop Handbook, 2nd ed. D. C. Ogden, editor. The Company of Biologists Ltd., Cambridge, UK. 361–387.
3. Simpson, I., B. Rose, and W. R. Loewenstein. 1977. Size limit of molecules permeating the junctional membrane channels. *Science.* 195: 294–296.
4. Schwarzmann, G., H. Wiegandt, B. Rose, A. Zimmerman, D. Ben-Haim, and W. R. Loewenstein. 1981. Diameter of the cell-to cell junctional membrane channels as probed with neutral molecules. *Science.* 213:551–553.
5. Flagg-Newton, J., I. Simpson, and W. R. Loewenstein. 1979. Permeability of the cell-to-cell membrane channels in mammalian cell junction. *Science.* 205:404–407.
6. Willecke, K., J. Eiberger, J. Degen, D. Eckardt, A. Romualdi, M. Güldenagel, U. Deutsch, and G. Söhl. 2002. Structural and functional diversity of connexin genes in the mouse and human genome. *Biol. Chem.* 383:725–737.
7. Elfgang, C., R. Eckert, H. Lichtenberg-Fraté, A. Butterweck, O. Traub, R. A. Klein, D. F. Hülser, and K. Willecke. 1995. Specific permeability and selective formation of gap junction channels in connexin-transfected HeLa cells. *J. Cell Biol.* 129:805–817.
8. Nicholson, B. J., P. A. Weber, F. Cao, H. Chang, P. Lampe, and G. Goldberg. 2000. The molecular basis of selective permeability of connexins is complex and includes both size and charge. *Braz. J. Med. Biol. Res.* 33:369–378.
9. Donaldson, P., R. Eckert, C. Green, and J. Kistler. 1997. Gap junction channels: new roles in disease. *Histol. Histopathol.* 12:219–231.
10. Goldberg, G. S., V. Valiunas, and P. R. Brink. 2004. Selective permeability of gap junction channels. *Biochim. Biophys. Acta.* 1662: 96–101.
11. Brink, P. R. 1996. Gap junction channel gating and permselectivity: their roles in co-ordinated tissue function. *Clin. Exp. Pharmacol. Physiol.* 23:1041–1046.
12. Veenstra, R. D. 1996. Size and selectivity of gap junction channels formed from different connexins. *J. Bioenerg. Biomembr.* 28: 327–337.
13. Gong, X.-Q., and B. J. Nicholson. 2001. Size selectivity between gap junction channels composed of different connexins. *Cell Commun. Adhes.* 8:187–192.
14. Cao, F. L., R. Eckert, C. Elfgang, J. M. Nitsche, S. A. Snyder, D. F. Hülser, K. Willecke, and B. J. Nicholson. 1998. A quantitative analysis of connexin-specific permeability differences of gap junctions expressed in HeLa transfectants and *Xenopus* oocytes. *J. Cell Sci.* 111:31–43.
15. Biegon, R. P., M. M. Atkinson, T. F. Liu, E. Y. Kam, and J. D. Sheridan. 1987. Permeance of Novikoff hepatoma gap junctions: quantitative video analysis of dye transfer. *J. Membr. Biol.* 96: 225–233.
16. Brink, P. R., and S. V. Ramanan. 1985. A model for the diffusion of fluorescent probes in the septate giant axon of earthworm: axoplasmic diffusion and junctional membrane permeability. *Biophys. J.* 48: 299–309.
17. Ramanan, S. V., and P. R. Brink. 1990. Exact solution of a model of diffusion in an infinite chain or monolayer of cells coupled by gap junctions. *Biophys. J.* 58:631–639.
18. Safranyos, R. G. A., and S. Caveney. 1985. Rates of diffusion of fluorescent molecules via cell-to-cell membrane channels in a developing tissue. *J. Cell Biol.* 100:736–747.
19. Miller, A. 1995. Quantitative junctional permeability measurements using the confocal microscope. *Microsc. Res. Tech.* 31:387–395.
20. Eckert, R., B. Adams, J. Kistler, and P. Donaldson. 1999. Quantitative determination of gap junctional permeability in the lens cortex. *J. Membr. Biol.* 169:91–102.
21. Weber, P. A., H.-C. Chang, K. E. Spaeth, J. M. Nitsche, and B. J. Nicholson. 2004. The permeability of gap junction channels to probes of different size is dependent on connexin composition and permeant-pore affinities. *Biophys. J.* 87:958–973.
22. Nitsche, J. M., H. C. Chang, P. A. Weber, and B. J. Nicholson. 2004. A transient diffusion model yields unitary gap junctional permeabilities from images of cell-to-cell fluorescent dye transfer between *Xenopus* oocytes. *Biophys. J.* 86:2058–2077.
23. Valiunas, V., E. C. Beyer, and P. R. Brink. 2002. Cardiac gap junction channels show quantitative differences in selectivity. *Circ. Res.* 91: 104–111.
24. Zimmerman, A. L., and B. Rose. 1985. Permeability properties of cell-to-cell channels: kinetics of fluorescent tracer diffusion through a cell junction. *J. Membr. Biol.* 84:269–283.
25. Marty, A., and E. Neher. 1983. Tight-seal whole-cell recording. *In* Single-Channel Recording, 1st ed. B. Sakmann and E. Neher, editors. Plenum Press. New York. 134–175.
26. Harris, A. L. 2001. Emerging issues of connexin channels: biophysics fills the gap. *Q. Rev. Biophys.* 34:325–472.
27. Traub, O., R. Eckert, H. Lichtenberg-Fraté, C. Elfgang, B. Bastide, K. H. Scheidtmann, D. F. Hülser, and K. Willecke. 1994. Immunochemical and electrophysiological characterization of murine connexin40 and -43 in mouse tissues and transfected human cells. *Eur. J. Cell Biol.* 64:101–112.
28. Trexler, E. B., F. F. Bukauskas, M. V. Bennett, T. A. Bargiello, and V. K. Verselis. 1999. Rapid and direct effects of pH on connexins revealed by the connexin46 hemichannel preparation. *J. Gen. Physiol.* 113:721–742.
29. Zimmerman, A. L. 1982. Kinetics of intracellular and cell-to-cell diffusion of fluorescent tracers. PhD thesis. University of Miami, Miami.
30. Verselis, V., R. L. White, D. C. Spray, and M. V. Bennett. 1986. Gap junctional conductance and permeability are linearly related. *Science.* 234:461–464.
31. Unger, V. M., N. M. Kumar, N. B. Gilula, and M. Yaeger. 1999. Three-dimensional structure of a recombinant gap junction membrane channel. *Science.* 283:1176–1180.
32. Unger, V. M., N. M. Kumar, N. B. Gilula, and M. Yaeger. 1997. Projection structure of a gap junction membrane channel at 7 Å resolution. *Nat. Struct. Biol.* 4:39–43.
33. Wang, H. Z., and R. D. Veenstra. 1997. Monovalent ion selectivity sequences of the rat connexin43 gap junction channel. *J. Gen. Physiol.* 109:491–507.
34. Guan, X. J., B. F. Cravatt, C. R. Ehring, J. E. Hall, D. L. Boger, R. A. Lerner, and N. B. Gilula. 1997. The sleep-inducing lipid oleamide deconvolutes gap junction communication and calcium wave transmission in glial cells. *J. Cell Biol.* 139:1785–1792.
35. Bukauskas, F. F., A. Bukauskiene, and V. K. Verselis. 2002. Conductance and permeability of the residual state of connexin43 gap junction channels. *J. Gen. Physiol.* 119:171–186.

36. Qu, Y., and G. Dahl. 2002. Function of the voltage gate of gap junction channels: selective exclusion of molecules. *Proc. Natl. Acad. Sci. USA.* 99:697–702.

37. Kwak, B. R., and H. J. Jongsma. 1996. Regulation of cardiac gap junction channel permeability and conductance by several phosphorylating conditions. *Mol. Cell. Biochem.* 157:93–99.

38. Ek-Vitorin, J. F., and J. M. Burt. 2005. Quantification of gap junction selectivity. *Am. J. Physiol. Cell Physiol.* 298:C1535–C1546.

39. Laird, D., M. Castillo, and L. Kasprzak. 1995. Gap junction turnover, intracellular trafficking, and phosphorylation of connexin43 in brefeldin A-treated rat mammary tumor cells. *J. Cell Biol.* 131:1193–1203.

40. Hu, X., M. Ma, and G. Dahl. 2006. Conductance of connexin hemichannels segregates with the first transmembrane segment. *Biophys. J.* 90:140–150.

41. Safranyos, R. G. A., S. Caveney, J. G. Miller, and N. O. Petersen. 1987. Relative roles of gap junction channels and cytoplasm in cell-to-cell diffusion of fluorescent tracers. *Proc. Natl. Acad. Sci. USA.* 84: 2272–2276.

42. Rae, J. L., C. Bartling, J. Rae, and R. T. Mathias. 1996. Dye transfer between cells of the lens. *J. Membr. Biol.* 150:89–103.

43. Christ, G. J., P. R. Brink, and S. V. Ramanan. 1994. Dynamic gap junctional communication: a delimiting model for tissue responses. *Biophys. J.* 67:1335–1344.